

Analysis of first four moderate geomagnetic storms of the 2015 year

Emre Eroglu (✉ eroglumre@gmail.com)



Kirklareli University

Full paper

Keywords: Solar wind (SW) parameters, Zonal geomagnetic (ZG) indices, Artificial neural network (ANN)

Posted Date: March 30th, 2021

DOI: <https://doi.org/10.21203/rs.3.rs-332486/v1>

License:   This work is licensed under a Creative Commons Attribution 4.0 International License. [Read Full License](#)

Version of Record: A version of this preprint was published at Arabian Journal of Geosciences on November 20th, 2021. See the published version at <https://doi.org/10.1007/s12517-021-08816-3>.

Abstract

This essay investigates of first four *moderate* geomagnetic activities (04 January storm, 07 January storm, 17 February storm, and 24 February storm) of 2015 in the 24th solar cycle. It tries to understand these storms with the aid of the zonal geomagnetic indices. It predicts the *zonal geomagnetic indices* (Dst, ap, AE) of the storms by an *artificial neural network model*. The phenomena that occurred in January and February are discussed on the *solar wind parameters* (B_z , E, P, N, v, T) and the zonal geomagnetic indices obtained from NASA. In the study, after glancing at the 2015-year general appearance, binary correlations of the variables are indicated by the covariance matrix, and the hierarchical cluster of the variables are presented by the dendrogram.

The artificial neural network model is governed by the physical principles in the paper. The model uses the solar wind parameters as *inputs* and the zonal geomagnetic indices as *outputs*. The causality principle forms the models by cause-effect association. Back propagation algorithm is specified as Levenberg–Marquardt (trainlm) and 35 neural numbers are utilized in the artificial neural network. The neural network model predicts the Dst, ap, and AE indices of January and February geomagnetic storms with an accuracy that deserves discussion. Estimating the geomagnetic activities may support interplanetary works.

Introduction

Natural events are interpreted by mathematicians via data. After these data are converted to variables, then the variables provide modeling opportunities to researchers. According to the physical conditions, the variables may be separated into dependent and independent ones. When the *solar wind* (SW) parameters are considered as independent variables, the *zonal geomagnetic* (ZG) indices are considered as dependent variables, as well. Geomagnetic activities (Akasofu, 1964; Kamide et al., 1998; Rathore et al., 2014) are also such natural events. This paper tries to understand and interpret the 04 January storm (Dst=-62 nT), 07 January storm (Dst=-99 nT), 17 February storm (Dst=-64 nT), and 24 February storm (Dst=-56 nT) *moderate* geomagnetic activities built on the (SW) parameters and the (ZG) indices depending on the cause (B_z , E, P, N, v, T)-effect (Dst, ap, AE) association. The storms are considered by the *artificial neural network* (ANN) model. In the ANN model, Levenberg–Marquardt (trainlm) is selected as the back-propagation (Rumelhart et al., 1986; Conway, 1998) algorithm and thirty-five neural numbers are utilized (Williams and Zipser, 1989; Elman, 1990 Gardner and Dorling, 1998; Fausett, 1994).

The sun is a plasma-dense energy and power source that makes durable magnetic waves. These magnetic waves are conveyed out to the interplanetary medium by the SWs. The SW has dense particles that energy induced spreading from the sun (Parker, 1958). Swallowing by *coronal mass ejection* (CME) cloud of the earth's magnetosphere-ionosphere and the orienting of the B magnetic field's B_z component from the positive northward to the negative southwards are invaluable for the geomagnetic storm. Shortly, the fast alteration in the magnetosphere of the earth governed by the SW scattering out of the sun is named a geomagnetic storm. CME is the burst of magnetically charged plasma into the interplanetary medium with high speeds. The dense magnetic field is burst in the solar corona (Lin and Ni, 2018) by direct CMEs in a loop through (magnetic) reconnections (Kamide et al., 1998; Gonzalez et al., 1989; Borovsky, 2012; Fu et al.,

2013; 2017). Polarized magneto sonic waves and CME straightly turn out the SW parameters (Gonzalez et al. 1999). One of the governor SW parameters is the magnetic field B_z component. The negative B_z magnetic field replaces from the northward to the southward. This orientation and decreasing negatively direction cause of the terrestrial magnetic field by causing disturbances with magnetic reconnections. Turbulences and fluctuations in the magnetic field controlled by the storm disturbance storm time index (Dst) (Dungey. 1961; Sugiura. 1964) from ZG indices can be called storm after the minimum peak B_z . Storms may be defined in 3-phases: The *initial phase* (sudden commencement), the *main phase*, and the *recovery phase*. In the initial phase, in which the storm begins, the Dst index decreases from positive values to negative values supporting the magnetic field. In the main phase, the Dst index indicates negative values. When the negative values show the minimum values, it is followed by the recovery phase. Lastly, the geomagnetic storm finishes with the recovery phase when the fluctuating in the magnetic field ends and the Dst index indicates to the initial values. In moderate storms, following the B_z parameter of the Dst index with a delay (Burton, 1975) of 5-6 hours is the response of the ring current to the SW. To better understand a geomagnetic storm (Mayaud 1980; 2011; Eroglu, 2018; Eroglu, 2019; Inyurt and Sekertekin, 2019; Inyurt, 2020; Koklu, 2020; Eroglu, 2020), the author considers to models between the SW parameters and the ZG indices. This paper utilizes hourly versions of the SW parameters and the ZG indices.

This essay tries to investigate 04 January, 07 January, 17 February, and 24 February (2015) storm based on their physical requirements via an ANN model by meticulously governing the causality principle (Eroglu, 2011; Eroglu et al., 2012a; 2012b, Eroglu, 2021). The ANN is a precious method; it may be utilized as an operative approach for forecasting in scientific disciplines (Elman, 1990; Gleisner et al., 1996; Boberg et al., 2000; Gleisner and Lundstedt, 2001; Karayiannis and Venetsanopoulos, 2013). ANN model(s) application has been remarking in current decades owing to its distinctives such as learning capability, adaptation to changes, and ease of tools.

Investigations of earth-sun interaction, geomagnetic activities (Gleisner et al., 1996; Boberg et al., 2000; Gleisner and Lundstedt, 2001), weather estimations, etc. with ANNs (Gardner and Dorling, 1998; Lundstedt et al., 2005; Pallochia et al., 2006) is effective in terms of space costs-times. ANN models founded by inferring geomagnetic storms' CMEs (Uwamahoro et al., 2012, Singh and Singh, 2016) give reasonable results with high forecasting ratio of storms. Long term time data ANN models involving SW parameters not only forecast the Dst index (Lundstedt, 1992; Lundstedt and Wintoft, 1994; Gleisner et al., 1996; Fenrich and Luhman, 1998; O'Brien and McPherron, 2000; Lundstedt et al., 2002; Bala, 2012; Uwamahoro, 2012; Singh and Singh, 2016) also estimates geomagnetic activities phases (Gleisner et al., 1996). One may see the trouble of the forecasting of the Dst index, without high-capacity computers with an 84% accuracy. At the '90s, such an amazing estimation has guided the new ANN models (Gleisner et al., 1996). The another ZG indicator Kp index is estimated by the SW parameters as the proton density (N), the flux velocity (v), and the B_z magnetic field. The Kp index ANN model displays a remarkable estimation ratio (Boberg et al., 2000; Lundstedt, 1992). The ap index significant model also utilizes the SW parameters as proton density and magnetic field (Altadill et al. 2001). The auroral electrojet index AE model uses the proton density (N), the flux density (v), and the magnetic field (B). One may realize from the ANN model estimation more than of 70% of the monitored the AE index (Gleisner and Lundstedt, 2001).

This paper investigates separately different moderate storms. Governing the ANN model by the SW parameters, the ZG indices shapes the investigation. In the examination of the first four moderate storm, the correlation matrix specifies binary relation of the variables, the dendrogram illustrates of the hierarchical cluster of the data. The events that visualized with graphics is exhibited to the reader. The SW scattering time from bow shock to magnetosphere-ionosphere are not considered in the study when it is utilized the ZG indices from ground stations.

After searching the literature by introduction, in Section 2 yearly ZG indices appearances are seen besides variables five-day scattering of them is announced. In Section 3 the ANN model and some properties of data are discussed. The paper is completed with a discussion in Section 4.

Data

SPEDAS is used in this essay. Before launching the first four moderate storms of the 2015 year (day by day), one needs a glance annual appearance of the ZG indices. One can find observed and estimated values of the 2015 year in Figure 1 besides their errors. The estimated Dst, ap, and AE indices average errors are 0.399, 0.271, 0.303 with values 0.953, 0.272, 0.243 their relative variance, respectively.

Geomagnetic storms are classified according to the strength of the Dst index (Loewe and Prölss 1997). If Dst index is between -50 nT and -30 nT then it is weak. When it is between -100 nT and -50 nT, then it is called moderate, and from -200 nT to -100 nT then it is named the strong (intense-severe) storm. Figure 2 is a 120-hour view of some data related to the activities. The storm day is placed in the middle of the five days.

It would be appropriate to discuss Figure 2' summary.

04 January 2015 Storm: On 04 January at 14:00 UT when the B_z magnetic field is at its minimum value of -8.8 nT, the Dst orients to -56 nT, the electric field E shows to its maximum value of 3.53 mV/m. Simultaneously, the proton density N signs to $6.9/\text{cm}^3$, the plasma flow speed v shows 401 km/s, and the pressure P reaches 2.63 nPa. As a response after two hours, at 16:00 UT, the Dst index and the auroral electrojet AE index hit the minimum-maximum peak values -62 nT and 866 nT, respectively.

On 03 January at 00:00 UT when the first CME is burst out to the interplanetary medium, instant instability of the dynamic pressure P reaches its maximum value of 8.36 nPa in addition to indicating to the proton density N maximum value of $33.0/\text{cm}^3$ and the flow speed v minimum value of 379 km/s.

07 January 2015 Storm: Four hours before, on 07 January at 07:00 UT, the Dst index indicates its peak value of -99 nT, the last CME is burst out. Meantime, the dynamic pressure P jumps from 6.05 nPa to its highest value of 12.36 nPa and the proton density N hits its maximum value of $29.4/\text{cm}^3$. After two hours, on 07 January at 9:00 UT the B_z magnetic field decreases to its minimum value (-17.04 nT), the electric field E ranges to its highest value of 8.16 mV/m, the AE index shows its maximum value of 1327 nT, and the ap ZG index hits its maximum value of 94 nT.

17 February 2015 Storm: In the five days discussion period, when the first CME is burst out on 15 February at 04:00 UT with the sudden commencement in the dynamic pressure P, then the proton density N peaks immediately its maximum value of 21.9 1/cm^3 . On 17 February at 21:00 UT, before three hours the Dst ZG index taking its minimum value of -62 nT, the magnetic field B_z component indicates its peak value of -12.0 nT and the electric field (E) hits its maximum value of 4.54 mV/m. After three hours, at 00:00 UT, the ap index, the AE index, and the Dst index indicate their maximum values of 48 nT, 579 nT, and -62 nT, respectively.

24 February 2015 Storm: In the five days storm discussion period, when the first CME is burst out on 23 February at 03:00 UT with the sudden commencement in the dynamic pressure P, then the proton density N hits immediately value of 20.3 1/cm^3 . After eight hours at 08:00 UT, when the second CME is burst out, the dynamic pressure (P) hits 5.46 nPa, the proton density (N) indicates 20.0 1/cm^3 . Within four hours the magnetic field B_z component hits its peak value of -7.7 nT (11:00 UT), the dynamic pressure (P) increases its maximum value of 8.81 nPa (12:00 UT), and the proton density (N) shows its maximum value of 31.7 1/cm^3 (at 12:00 UT).

Modeling

Binary relationships with correlation matrix for the data of moderate 04 and 07 January, 17 and 24 February storms are indicated in Table 1a and 1b. The Pearson correlation matrix shows the relationship of variables. When the constants in Table 1a and 1b are close to ± 1 , mutual correlation strengthens. Dendrogram of these moderate storms variables and scattering of data are specified in Figure 3a, 3b, Figure 4, respectively.

Table 1a Correlation of data

	04 January 2015									07 January 2015								
	B_z	T	N	v	P	E	Dst	ap	AE	B_z	T	N	v	P	E	Dst	ap	AE
(nT)	1	.230*	-.246**	.492**	-.134	-.996**	.346**	-.331**	-.669**	1	.165	-.081	-.150	-.116	-.999**	.122	-.412**	-.577**
(K)		1	-.263**	.596**	-.083	-.205*	-.242**	-.009	-.145		1	-.417**	.508**	-.321**	.149	.057	-.238**	-.080
1/cm^3)			1	-.568**	.932**	.221*	-.042	.426**	.349**			1	-.244**	.986**	.091	-.085	.657**	.297**
(m/s)				1	-.366**	-.452**	.089	-.344**	-.424**				1	-.108	.136	.162	-.066	.100
(nPa)					1	.119	-.021	.395**	.298**					1	.123	-.063	.657**	.311**
(mV/m)						1	-.319**	.308**	.635**						1	-.138	.415**	.585**
(nT)							1	-.618**	-.654**							1	-.291**	-.540**
(nT)								1	.628**								1	.701**
(nT)									1									1

Table 1b Correlation of data

17 February 2015										24 February 2015									
	B _z	T	N	v	P	E	Dst	ap	AE	B _z	T	N	v	P	E	Dst	ap	AE	
(nT)	1	.326**	.027	-.201*	-.120	-.997**	.522**	-.513**	-.630**	1	.087	-.214*	.370**	-.057	-.993**	-.215*	-.043	-.084	
(K)		1	.307**	.389**	.656**	.326**	-.439**	.590**	.516**		1	-.028	.677**	.395**	-.039	-.779**	.751**	.692**	
/cm ³)			1	-.431**	.826**	-.036	.342**	.110	.031			1	-.414**	.875**	.198*	-.022	.364**	.355**	
m/s)				1	.118	.216*	-.762**	.376**	.346**				1	.038	-.332**	-.639**	.272**	.239**	
nPa)					1	.117	-.122	.415**	.283**					1	.069	-.384**	.605**	.573**	
V/m)						1	-.532**	.525**	.628**						1	.176	.075	.104	
t(nT)							1	-.663**	-.644**							1	-.631**	-.698**	
(nT)								1	.648**								1	.743**	
(nT)									1									1	

** . Correlation is significant at the 0.01 level (2-tailed).

* . Correlation is significant at the 0.05 level (2-tailed).

After the mathematical introductory discussion, it can be appropriate to remember the frame of the model of an ANN. The ANNs have inspired from the working principles of the human brain. This complicated and trainable neural system, which is shaped by linking many neurons with several interface levels, imitates the brain. Studies firstly have involved to model neurons in the human brain mathematically. With increasing awareness, the ANN has become a scientific discipline today and it has been used in many different fields. The ANN, which observes information and data in different structures and procedures by recognizing them very rapidly, can reveal unknown and difficult to notice correlation between data. It permits modeling without the necessity for any preparation or info among inputs and outputs (Elman, 1990). Basically, inputs and corresponding outputs are specified to the network (Figure 5).

Training or educating of the ANN is provided by learning the relationship between input-output. This approach, called instructional learning, is a common approach (Peng et al., 1992). As an architectural configuration involving of some layers, the ANN uses data with a pre-determined number of artificial neural cells. The initial layer is generally the *input layer*. This layer is usually not numbered owing to the lack of weight factors and initiation functions of the inputs in the input layer. The second mid-layers, called the *hidden layer*, can be founded so many as needed. Using one hidden layer (Elman, 1990; El-Din & Smith, 2002) is usual besides researchers to change into more than one hidden layer for adapting the target function. The layer called the *output layer* is the last layer. In this paper, the estimations are completed by the *back propagation* (Rumelhart et al., 1986) ANN algorithm. The typical back propagation algorithm applying a feedback learning structure is the gradient descent algorithm that moves the network weights in the direction of the negative gradient of the performance function. Many backpropagation algorithms appropriate for nearly all problem in ANNs are driven by standard optimization methods such as gradient descent and the Newton approach (Lipmann, 1987). Feedback learning using continuous input diminishes the error caused by backward agglomeration. The author utilizes the widely performed Levenberg–Marquardt (trainlm) learning algorithm.

After the creation of the learning algorithm, the number of neurons of the hidden layer have to be specified. The number of neurons should be determined as needed. Too few neurons cause the pattern unable to be learned by the network, and a large number of neurons cause memorizing by the network, as well. A small

enough number of neurons forces the ANN to improve *generalization* facility (Stern, 1996). In the paper, the hidden layers' neurons numbers are determined to be thirty-five. In this neuron number, the mean square error (MSE) value begins to indicate no substantial change.

The work consists of three layers: The input layer, hidden layer, and output layer (Figure 5). In harmony with the causality principle, the SW parameters (B_z , E, P, N, v, T) are variables of the input layer and the ZG indices (Dst, ap, AE) are variables of the output layer. For the ANN model to be able to learn well without memorizing, the *sigmoid transfer function* is selected as the neural transition function (Fausett, 1994). A *Linear transfer function* is used in the output layer. Where a total of 120 (five days) data is investigated, 84 data are utilized for *training* ANN (70%), 12 data for *validation* (10%) and 24 data for *testing* (20%) (Haykin 1994).

As it may be realized from Figure 6a, the MSE values do not change after 6 updates (step, epoch) for the Dst index, after 8 updates for the ap index, and after 8 updates for the AE index in the 04 January storm (left column). In addition to this, the MSE values do not change after 7 updates for the Dst index, after 8 updates for the ap index, and after 8 updates for the AE index in the 07 January storm (right column). Therefore, learning (training) is finished. Up to these iteration totals, where the best verification performance happens, there is no monitoring of memorization owing to error constancy. Because the validation and test set errors show similar behavior and no substantial memorization happens, the network performance is acceptable.

One can see from Figure 6b, the MSE values do not change after 7 updates (step, epoch) for the Dst index, after 7 updates for the ap index, and after 6 updates for the AE index in the 17 February storm (left column). In addition to this, the MSE values do not change after 8 updates for the Dst index, after 8 updates for the ap index, and after 8 updates for the AE index in the 24 February storm (right column).

Figures 7a, 7b, and Figure 8a, b, c visualizes the results of the discussion. In the Figure 7a and 7b, the Dst, ap, AE indices line up from the top to the bottom, respectively. While Figure 7a and 7b displays the correlation, Figure 8a, b, c exhibits the character of observed, forecasted values with their errors. Graphically, forecasting consequences are in Figures 7a, 7b between the output and the target (the Dst, ap, AE indices).

In the literature, the significant studies in the literature have reached remarkable consequences in the estimation of the Dst, the ap (or the Kp), the AE index. In the Dst ZG index estimations, Gleisner et al. (1996) with 84%, Fenrich and Luhman (1998) with 79%, O'Brien and McPherron (2000) with 88%, Lundstedt et al. (2002) with 88%, Pallochia et al. (2006) with 90%, Bala and Reiff (2012) with 86%, Uwamahoro et al. (2012) with 86% (for severe storms 100%), Singh and Singh (2016) with 79%, Balan et al. (2017) with 100% have accomplished their discussions.

In the Kp ZG index estimations, Boberg et al. (2000) with 77%, Wing et al. (2005) with 94%, Bala and Reiff (2012) with 96%, Young et al. (2013) with 93%, Solares et al. (2016) with 91%, Wintoft et al. (2017) with 92% have declared their discussions.

In the AE index estimations, Gleisner et al. (1996) with more than 70%, Takalo and Timonen (1997) with 98%, Gleisner and Lundstedt (2001) with 84%, Bala and Reiff (2012) with 83% have accomplished their

discussions.

For the 04 January: The Dst, ap, and AE indices estimation models are 98.5%, 98.1%, and 98.3% (Figure 7a-left column) reliable, respectively.

For the 07 January Storm: The Dst, ap, and AE indices estimation models are 98.8%, 98.5%, and 98.4% (Figure 7a-right column) reliable, respectively.

For the 17 February Storm: The Dst, ap, and AE indices estimation models are 97.6%, 98.9%, and 98.6% (Figure 7b-left column) reliable, respectively.

For the 24 February Storm: The Dst, ap, and AE indices estimation models are 98.9%, 98.5%, and 98.6% (Figure 7b-right column) reliable, respectively.

Four moderate storm forecasting model outcomes look similar. It is obvious that the ANN model displays the reliable method and the fit output for these moderate geomagnetic activities.

The illustration of the estimated Dst, ap, AE index values and their errors of 04 January moderate storm with actual ones from NASA is exhibited in Figure 8a, respectively. In Figure 1 and Figure 8a, b, c one can see the *error* ratio in the comparison of the estimated-observed values of the Dst, ap, and AE indices. The *error* between

the real-forecasted ZG indices values can be observed with the $Error = \left| \frac{Dst_{est} - Dst}{Dst} \right|$, $Error = \frac{|ap_{est} - ap|}{ap}$, and $Error = \frac{|AE_{est} - AE|}{AE}$, where the Dst_{est} , ap_{est} , and AE_{est} are the estimated Dst, ap, and AE index values, respectively. Low error shows the strength and accuracy of the estimation.

According to Figure 8a, the estimated Dst index average errors are 0.034, 0.009, 0.389, 0.064 with values 0.011, 0.002, 0.841, 0.012 their relative variance, respectively.

The illustration of the forecasted ap index values and their errors all of storms with actual ones from NASA is exhibited in Figure 8b, respectively.

According to Figure 8b, the estimated ap index average errors are 0.198, 0.265, 0.035, 0.019 with values 0.047, 0.143, 0.003, 0.001 their relative variance, respectively.

The comparison of the estimated AE index values and their errors all of storms with actual ones from NASA is displayed in Figure 8c, respectively.

According to Figure 8c, the estimated AE index average errors are 0.444, 0.022, 0.219, 0.215 with values 0.340, 0.018, 0.111, 0.056 their relative variance, respectively.

The effect of variables (for solar wind parameters) on the ANN model (Gontarski et al., 2000) can be specified with the formula **% Effect = 100 · (1 - R_n / R_{diff})** by omitting these variables from the investigation process. The correlation coefficients govern this formula. In the formula; R_n is the correlation coefficient

attained by excluding input. R_{dif} is the basic correlation coefficient between estimated and observed values. Table 2a and 2b exhibits the effect of variables on the ANN model.

Table 2a Effect of each variable on the performance of ANN estimation

04 January Storm							07 January Storm						
Variable	Dst(nT)		ap(nT)		AE(nT)		Variable	Dst(nT)		ap(nT)		AE(nT)	
	R	Effect on R (%)	R	Effect on R (%)	R	Effect on R (%)		R	Effect on R (%)	R	Effect on R (%)	R	Effect on R (%)
Basic Value	0.985	-	0.981	-	0.983	-	Basic Value	0.988	-	0.985	-	0.984	-
B_z (nT)	0.950	3.54	0.838	14.66	0.864	12.16	B_z (nT)	0.889	10.02	0.885	10.25	0.888	9.76
T(K)	0.982	0.21	0.977	0.71	0.982	0.11	T(K)	0.980	0.81	0.966	1.92	0.982	0.20
$N(1/cm^3)$	0.910	10.37	0.899	8.40	0.938	4.60	$N(1/cm^3)$	0.901	8.81	0.814	17.32	0.855	13.11
$v(km/s)$	0.850	13.70	0.894	8.91	0.915	6.94	$v(km/s)$	0.885	10.53	0.827	16.04	0.890	9.55
P(nPa)	0.892	9.43	0.857	12.64	0.967	1.63	P(nPa)	0.866	12.35	0.886	10.05	0.982	0.20
E(mV/m)	0.982	0.20	0.968	1.33	0.968	1.53	E(mV/m)	0.979	0.91	0.981	0.41	0.973	1.12

Table 2b Effect of each variable on the performance of ANN estimation

17 February Storm							24 February Storm						
Variable	Dst(nT)		ap(nT)		AE(nT)		Variable	Dst(nT)		ap(nT)		AE(nT)	
	R	Effect on R (%)	R	Effect on R (%)	R	Effect on R (%)		R	Effect on R (%)	R	Effect on R (%)	R	Effect on R (%)
Basic Value	0.976	-	0.989	-	0.986	-	Basic Value	0.989	-	0.985	-	0.986	-
B_z (nT)	0.909	6.86	0.889	10.11	0.913	7.40	B_z (nT)	0.758	23.36	0.906	8.02	0.915	7.20
T(K)	0.971	0.51	0.978	1.11	0.982	0.41	T(K)	0.980	0.91	0.983	0.20	0.983	0.21
$N(1/cm^3)$	0.903	7.48	0.883	10.72	0.919	6.80	$N(1/cm^3)$	0.908	8.19	0.807	18.10	0.871	11.66
$v(km/s)$	0.896	8.20	0.900	9.00	0.909	7.73	$v(km/s)$	0.909	8.03	0.861	12.59	0.916	7.10
P(nPa)	0.907	7.07	0.892	9.81	0.980	0.61	P(nPa)	0.860	13.04	0.912	7.41	0.982	0.41
E(mV/m)	0.971	0.51	0.969	2.02	0.971	1.52	E(mV/m)	0.986	0.30	0.964	2.23	0.984	0.20

04 January Storm: In the modeling of the Dst (nT) index forecasting, the plasma flow speed v (km/s) indicates the main effect. The correlation coefficient diminishes by 13.70% when neglecting the plasma flow speed (Table 2a). The second-high effect belongs to the proton density N ($1/cm^3$) and dynamic pressure P (nPa). The correlation coefficient weakens by 10.37% and 9.43% when omitting the proton density and dynamic pressure P value, respectively (Table 2a). Finally, when ignoring the magnetic field B_z (nT) component, the Dst index is affected by 3.54%. The plasma flow speed v (km/s), the proton density N ($1/cm^3$), the dynamic pressure P (nPa), and the magnetic field B_z (nT) are indispensable estimators for the

Dst (nT) index (Burton et al., 1975; Gleisner et al., 1996). Physically, coronal holes created by the instability of hot particles is the origin of the flow speed v (km/s). The SW streams have high-speed. The polarization of the magnetic field is indicated by the parameters of the SW speed (Tsurutani et al., 2006). Besides orienting the magnetic field B_z (nT) component from southward to northward and indicating its negative values, the flow speed v (km/s) is shaped the geomagnetic storm. The flow speed v (km/s) and the B_z (nT) component, with these anomalous replies, show that the Dst (nT) index should decline to negative minimum. With enhancing the proton density N ($1/\text{cm}^3$), the high-density plasma dynamic pressure P (nPa), and SW suppress the magnetosphere (Tsurutani et al., 2006). The reflection of the disturbance caused by this compress governed by the flow speed v (km/s) is the Dst (nT) index. Accordingly, one of the principal motivations why the Dst (nT) index inclines to minimums is the flow speed (Gonzalez et al., 1989; Borovsky, 2012; Borovsky and Yakymenko, 2017). The ANN model that shapes the Dst values prediction agrees with the literature (Table 2a and 2b).

The maximum impact on the ap (nT) index forecasting regards the magnetic field B_z (nT) component, the dynamic pressure P (nPa), the flow speed v (km/s), and proton density N ($1/\text{cm}^3$). When the magnetic field and the dynamic pressure are neglected, the correlation ratio declines by 14.66% and 12.64%, respectively (Table 2a). The flow speed v (km/s) and the proton density N ($1/\text{cm}^3$) are also other high parameters for the ap index. If these variables are omitted from the ap forecasting, the model correlation constant diminishes by 8.91% and 8.40%, respectively. Physically, the magnetic field polarizations indicate parallel effects with the dynamic pressure P (nPa), the flow speed v (km/s), and the proton density N ($1/\text{cm}^3$) while the ap index nonlinearly responses to the instabilities (Altadill et al. 2001; Eroglu, 2018; 2019; 2020; 2021; Inyurt, 2020; Koklu, 2020). The noticeable relation between B_z (nT) magnetic field, the dynamic pressure P (nPa), the flow speed v (km/s), and proton density N ($1/\text{cm}^3$) and the ap (nT) index may be perceived in Table 2a.

In the ANN estimation model for the AE (nT) index, the highest impact relates with magnetic field B_z (nT) component. One may see when neglecting the B_z (nT) magnetic field, the correlation constant decreases by 12.16% (Table 2a). The magnetic field is accompanied by the flow speed v (km/s) and proton density N ($1/\text{cm}^3$) during the calculation of the AE (nT) index correlation ratio. It is realized that the value of R declines by 6.94% and 4.60% when the flow speed v (km/s) and proton density N ($1/\text{cm}^3$) are subtracted from the ANN model of the AE index, respectively (Table 2a) (Gleisner and Lundstedt, 2001).

07 January Storm: Parallel conclusions can also be realized in 07 January moderate storm. In the demonstrating of the Dst index estimation, the highest effect belongs to the dynamic pressure P (nPa), the flow speed v (km/s), and the B_z (nT) magnetic field. The correlation coefficient diminishes by 12.35%, 10.53%, and 10.02% when neglecting the mentioned SW parameters value, respectively (Table 2a). According to Table 2a, the proton density N ($1/\text{cm}^3$) affects the Dst (nT) index with a value of 8.81%.

The maximum impact on the ap (nT) index forecasting regards the proton density N ($1/\text{cm}^3$) and the flow speed v (km/s). When the proton density and the flow speed are omitted, the correlation constant value decreases by 17.32% and 16.04%, respectively (Table 2a). Secondly, the other main factors are the B_z

magnetic field (nT) and the dynamic pressure P (nPa) for the ap (nT) index. If they are omitted from the ap (nT) forecasting, the model correlation ratio decreases by 10.25% and 10.05%, respectively (Table 2a).

In the discussion for the estimation of the AE (nT) index, the highest effect belongs to the proton density N ($1/\text{cm}^3$). One can perceive when neglecting the proton density, the correlation constant value decreases by 13.11% (Table 2a). Besides the proton density, it is perceived that the value of R decreases by 9.76% and 9.55% when the magnetic field B_z (nT) component and the flow speed v (km/s) are subtracted from the AE index model, respectively (Table 2a).

17 February Storm: This moderate storm also reflects similar effects. The Dst (nT) index estimation responds to neglect the flow speed v (km/s), the proton density N ($1/\text{cm}^3$), the dynamic pressure P (nPa), and the B_z (nT) magnetic field. The correlation constant decreases by 8.20%, 7.48%, 7.07%, and 6.86% when neglecting mentioned SW parameters value, respectively (Table 2b).

The maximum effect on the ap (nT) index estimation regards the proton density N ($1/\text{cm}^3$), the B_z magnetic field (nT), the dynamic pressure P (nPa), and the flow speed v (km/s). When the mentioned SW parameters are omitted, the correlation constant value decreases by 10.72%, 10.11%, 9.81%, and 9.00%, respectively (Table 2b).

In the discussion for the estimation of the AE (nT) index, the highest effect belongs to the flow speed v (km/s), the magnetic field B_z (nT) component, and proton density N ($1/\text{cm}^3$). One can realize when neglecting these parameters, the correlation constant value decreases by 7.73%, 7.40%, and 6.80%, respectively (Table 2b).

24 February Storm: Eventually, according to 24 February moderate storm, demonstrating of the Dst (nT) index estimation is deeply related to the B_z (nT) magnetic field, the dynamic pressure P (nPa), the proton density N ($1/\text{cm}^3$), and the flow speed v (km/s). The correlation coefficient diminishes by 23.36%, 13.04%, 8.19%, and 8.03% when neglecting these SW parameters, respectively (Table 2b).

The maximum impact on the ap (nT) index estimation regards the proton density N ($1/\text{cm}^3$), the flow speed v (km/s), the B_z magnetic field (nT), and the dynamic pressure P (nPa). When the mentioned SW parameters are omitted, the correlation constant value decreases by 18.10%, 12.59%, 8.02%, and 7.41%, respectively (Table 2b). Secondly, the other factor is the electric field E (mV/m) for the ap (nT) index by affecting 2.23% (Table 2b).

In the discussion for the estimation of the AE (nT) index, the highest effect is observed by means of the proton density N ($1/\text{cm}^3$), the B_z (nT) magnetic field, and the flow speed v (km/s). One can perceive when neglecting these SW parameters, the correlation constant value decreases by 11.66%, 7.20%, and 7.10%, respectively (Table 2b).

Conclusion

The purpose of the study is to assess the four moderate geomagnetic storms that occurred in 2015 year. After glancing at the 2015 year as a whole, these first four moderate activities' zonal geomagnetic (ZG) indices are estimated efficiently. When the estimation of geomagnetic storms by the artificial neural network (ANN) compares with the literature, the conclusions are satisfactory.

For these events, it is notable that the ANN model estimates the zonal geomagnetic (ZG) indices over the solar wind (SW) parameters. A geomagnetic storm strength and its phases may be evaluated by discussing the ZG indices. The paper is based on the method of inputting the SW parameters to the ANN model and yielding the ZG indices as output. The forecasting performance that is agreed with the literature of the ANN model, whose outputs are the ZG indices, is acceptable. The results demonstrate that the model is over 90% consistent in the estimation of these four moderate storms' ZG indices. The essay, in addition to the estimation, handles for these storms the effect of the SW variables on the ANN model, too.

In accordance with the 04 January storm ANN model, for the Dst index, the flow speed (v), the proton density (N), and the dynamic pressure (P) have a high effect, the magnetic field (B_z) component has the moderate effect. Furthermore, the magnetic field (B_z), the dynamic pressure (P), the flow speed (v) with the proton density (N) affect the ap index highly. For the auroral electrojet index AE, the magnetic field (B_z) has a high effect, the flow speed (v) and the proton density (N) have a moderate effect.

According to the 07 January moderate storm ANN model, for the Dst index, the dynamic pressure (P), the flow speed (v), the magnetic field (B_z), and the proton density (N) has a high effect. Moreover, the proton density (N), the flow speed (v), the magnetic field (B_z) with the dynamic pressure (P) affect the ap index highly. For the AE index, the proton density (N), the magnetic field (B_z), and the flow speed (v) have a high effect.

In accordance with the 17 February storm ANN model, for the Dst index, the flow speed (v), the proton density (N), the dynamic pressure (P), and the magnetic field B_z component has a high effect. Additionally, the proton density (N), the magnetic field (B_z), the dynamic pressure (P) with the flow speed (v) affect the ap index highly. The electric field (E) has also a moderate effect on the ap ZG index. In calculating auroral electrojet index AE, the flow speed (v), the magnetic field (B_z), and the proton density (N) have a high effect.

According to the ANN estimation model of the 24 February moderate storm, for the Dst ZG index, the magnetic field (B_z) has a very high effect and the dynamic pressure (P), the proton density (N), the flow speed (v) have a high effect. Furthermore, for the ap ZG index, the proton density (N) has a very high effect and the flow speed (v), the magnetic field (B_z), the dynamic pressure (P) have a high effect besides the moderate effect of the electric field (E). For the AE index, the proton density (N), the magnetic field (B_z), and the flow speed (v) have a high effect.

The harmony of the consequences of this study and the agreement with the previous discussions indicates that the reliability of the paper's results. The author expects to contribute to geomagnetic storm estimations by making it easier to understand their dynamics. The forecasted Dst, ap, and AE indices for these storms can also be predicted for other storms. With a similar approach, it will not be difficult for the ANN model to estimate the ZG indices not studied in this discussion for weak, moderate, or severe storms. The indices

considered together with the SW parameters prepare the ground for predictable storms. The author hopes to attain the same results for weak, moderate, and severe storms in the next discussions.

Declarations

Acknowledgements

The author presents his respects to NASA and Kyoto University.

Authors' contributions

This essay has one author. He approves the last version of the essay.

Funding

We declare no funding.

Availability of data

The data set in this essay are available from the corresponding author on demand.

Competing interests

The author declares no competing interest.

References

Akasofu, S.I., "The development of the auroral substorm" *Planet. Space Sci.*, 12(4) (1964): 273-282, [https://doi.org/10.1016/0032-0633\(64\)90151-5](https://doi.org/10.1016/0032-0633(64)90151-5)

Altadill, D., Apostolov, E.M., Sole, J.G., Jacobi, C.H., "Origin and development of vertical propagating oscillations with periods of planetary waves in the ionospheric F region", *Solar, Terrestrial and Planetary Science*, 26(6) (2001): 387-393, [https://doi.org/10.1016/S1464-1917\(01\)00019-8](https://doi.org/10.1016/S1464-1917(01)00019-8)

Bala, R and Reiff, P., "Improvements in short-term forecasting of geomagnetic activity", *Space Weather* 10(6) (2012): <https://doi.org/10.1029/2012SW000779>

Balan, N., Ebihara, Y., Skoug, R., Shiokawa, K., Batista, I. S., Tulasi Ram, S., Omura, Y., Nakamura, T., Fok, M.C., "A scheme for forecasting severe space weather", *Journal of Geophysical Research: Space Physics* 122(3) (2017): 2824–2835. <https://doi.org/10.1002/2016JA023853>

Boberg, F., Wintoft, P., Lundstedt, H., "Real time Kp predictions from solar wind data using neural networks", *Physics and Chemistry of the Earth, Part C: Solar, Terrestrial & Planetary Science* 25(4) (2000): 275-280, [https://doi.org/10.1016/S1464-1917\(00\)00016-7](https://doi.org/10.1016/S1464-1917(00)00016-7)

Borovsky, J.E., "The velocity and magnetic field fluctuations of the solar wind at 1 AU: Statistical analysis of Fourier spectra and correlations with plasma properties", *Journal of Geophysical Research: Space Physics* 117 (A5) (2012): A05104, doi: 10.1029/2011JA017499

Borovsky, J.E. and Yakymenko, K., "Systems science of the magnetosphere: Creating indices of substorm activity, of the substorm-injected electron population, and of the electron radiation belt", *Journal of Geophysical Research: Space Physics* 122(10) (2017): 10012-10035, doi: 10.1002/2017JA024250

Burton R. K., McPherron R. L., Russell C. T., "An empirical relationship between interplanetary conditions and Dst", *Journal of Geophysical Research* 80(31) (1975): 4204-4214, <https://doi.org/10.1029/JA080i031p04204>

Conway, A.J., "Time series, neural networks and the future of the Sun", *New Astronomy Reviews* 42 (5) (1998): 343–394, [https://doi.org/10.1016/S1387-6473\(98\)00041-4](https://doi.org/10.1016/S1387-6473(98)00041-4)

Dungey, J.W., "Interplanetary magnetic field and the auroral zones", *Physical Review Letters* 6 (1961): 47. <https://doi.org/10.1103/PhysRevLett.6.47>

EIDin, A. G., Smith, D.W. "A neural network model to predict the wastewater inflow incorporating rainfall events", *Water Research* 36(5) (2002): 1115–1126.

Elman, J.L., "Finding structure in time", *Cognitive Science* 14 (1990): 179.

Eroglu, E., "Dalga Kılavuzları Boyunca Geçici Sinyallerin Transferi", Ph.D. Thesis, Gebze High Technology Institute, 2011.

Eroglu, E., Aksoy, S., Tretyakov, O.A., "Surplus of energy for time-domain waveguide modes", *Energy Educ. Sci. Tech.*, 29(1) (2012): 495. (a)

Eroglu, E., Ak, N., Koklu, K., Ozdemir, Z., Celik, N., Eren, N., "Special functions in transferring of energy; a special case: "Airy function", *Energy Educ. Sci. Tech.*, 30(1) (2012): 719. (b)

Eroglu, E., "Mathematical modeling of the moderate storm on 28 February 2008", *New Astronomy* 60 (2018): 33, <https://doi.org/10.1016/j.newast.2017.10.002>

Eroglu, E., "Modeling the superstorm in the 24th solar cycle", *Earth Planets Spaces* 71:26 (2019), doi: <https://doi.org/10.1186/s40623-019-1002-1>

Eroglu, E., "Modeling of 21 July 2017 geomagnetic storm", *Journal of Engineering Technology and Applied Sciences* 5(1) (2020): 33, doi: 10.30931/jetas.680416

Eroglu, E., "Zonal geomagnetic indices estimation of the two super geomagnetic activities of 2015 with the artificial neural networks", *Advances in Space Research*. (Submitted)

Fausett, L.V., 1994. *Fundamentals of Neural Networks: Architecture, Algorithms and Applications*. Prentice-Hall, Inc, Englewood Cliffs, NJ.

- Fenrich, F.R. and Luhmann, J.G., "Geomagnetic response to magnetic clouds of different polarity", *Geophysical Research Letters*, 25(15) (1998): 2999–3002, <https://doi.org/10.1029/98GL51180>
- Fu, H.S., Yu. V. Khotyaintsev, A. Vaivads, A. Retinò and André, M., "Energetic electron acceleration by unsteady magnetic reconnection", *Nature Physics* 9 (2013):426-430, doi:10.1038/nphys2664
- Fu, H.S, Vaivads, A., Khotyaintsev, Y.V., André, M., Cao, J.B., Olshevsky, V.J., Eastwood, P., Retinò A., "Intermittent energy dissipation by turbulent reconnection ", *Geophysical Research Letters* 44(1) (2017): 37-43, doi:10.1002/2016GL071787
- Gardner, M.W. and Dorling, S.R, "Artificial neural networks (the multilayer perceptron)—a review of applications in the atmospheric sciences", *Atmospheric Environment* 32(14-15) (1998): 2627-2636, [https://doi.org/10.1016/S1352-2310\(97\)00447-0](https://doi.org/10.1016/S1352-2310(97)00447-0)
- Gleisner, H., Lundstedt, H., Wintoft, P., "Predicting geomagnetic storms from solar-wind data using time-delay neural networks", *Annales Geophysicae* 14 (1996): 679-866.
- Gleisner, H. and Lundstedt, H., "Auroral electrojet predictions with dynamic neural networks", *Journal of Geophysical Research Space Physics* 106(A11) (2001): 24541-24549, <https://doi.org/10.1029/2001JA900046>
- Gontarski, C.A., Rodrigues, P.R., Mori, M., Prenem, L.F., "Simulation of an industrial wastewater treatment plant using artificial neural networks", *Computers & Chemical Engineering*, 24(2) (2000): 1719-1723.
- Gonzalez, W.D. Tsurutani, B.T., Gonzalez, A.L.C., Smith, E.J., Tang, F., Akasofu, S.I., "Solar wind-magnetosphere coupling during intense magnetic storms (1978-1979)", *Journal of Geophysical Research* 94(A7) (1989): 8835, doi: 10.1029/ja094ia07p08835
- Gonzalez, W.D., Tsurutani, B.T., Gonzalez, A.L., "Interplanetary origin of geomagnetic storms", *Space Science Reviews* 88 (1999): 529-562, <https://doi.org/10.1023/A:1005160129098>
- Haykin, S., *Neural Networks-A Comprehensive Foundation*, Macmillan College Publ. Comp., Inc., New York, 1994.
- Inyurt, S., and Sekertekin, A., "Modeling and predicting seasonal ionospheric variations in Turkey using artificial neural network (ANN)", *Astrophysics and Space Science* 364(4) (2019): 62.
- Inyurt, S., "Modeling and comparison of two geomagnetic storms" *Advances in Space Research* 65(3) (2020): 966, <https://doi.org/10.1016/j.asr.2019.11.004>
- Kamide, Y., Baumjohann, W., Daglis, L.A., Gonzalez, W.D., Grande, M., Joselyn, J.A., McPherron, R.L., Phillips, J.L., Reeves, G.D., Rostoker, G., Shanna, A.S., Singer, H.J., Tsurutani, B.T., Vasyliuna V.M., "Current understanding of magnetic storms' Storm-substorm relationships", *Journal of Geophysical Research* 103(A8) (1998): 17705.

- Karayiannis, N., Venetsanopoulos, A.N., "Artificial neural networks: Learning algorithms, performance evaluation, and applications. Springer Science & Business Media 209 (2013): 373.
- Koklu, K, "Mathematical analysis of the 09 March 2012 intense storm", *Advances in Space Research* 66(4) (2020): 932, <https://doi.org/10.1016/j.asr.2020.04.053>
- Lin J. and Ni L. 2018, *Electric Currents in Geospace and Beyond*, Geophysical Monograph 235, 1th eds. John Wiley & Sons Inc.
- Lippmann, R.P., "An introduction to computing with neural nets", *ASSP Magazine, IEEE* 4 (2) (1987): 4-22.
- Loewe C.A. and Prölss, G.W., "Classification and mean behavior of magnetic storms", *Journal of Geophysical Research* 102(A7) (1997): 14209.
- Lundstedt, H., "Neural networks and predictions of solar-terrestrial effects" *Planet. Space Science* 40(4) (1992): 457-464, doi: 10.1016/0032-0633(92)90164-J
- Lundstedt, H. and Wintoft, P., "Prediction of geomagnetic storms from solar wind data with the use of a neural network", *Annales Geophysicae* 12 (1994): 19-24, <https://doi.org/10.1007/s00585-994-0019-2>
- Lundstedt, H., Gleisner, H. and Wintoft, P. "Operational forecasts of the geomagnetic Dst index", *Geophysical Research Letters* 29(24) (2002): 2181, <https://doi.org/10.1029/2002GL016151>
- Lundstedt, H., Liszka, L. and Lundin, R., "Solar activity explored with new wavelet methods", *Ann. Geophys.* 23 (2005): 1505–1511, doi: 10.5194/angeo-23-1505-2005
- Mayaud, P.N., "Derivation, Meaning, and Use of Geomagnetic Indices", *Geophys. Monogr. Ser.* 22 (1980): 154, doi: 10.1029/GM022
- O'Brien, T.P. and McPherron R.L., "Forecasting the ring current index Dst in real time", *Journal of Atmospheric and Solar-Terrestrial Physics* 62(14) (2000): 1295–1299, [https://doi.org/10.1016/S1364-6826\(00\)00072-9](https://doi.org/10.1016/S1364-6826(00)00072-9)
- Pallochia, G., Amata, E., Consolini, G., Marcucci, M.F. and Bertello, I. "Geomagnetic Dst index forecast based on IMF data only", *Ann. Geophys.* 24 (2006) 989–999, doi:10.5194/angeo-24-989-2006.
- Parker, E.N., "Dynamics of the interplanetary gas and magnetic fields", *Astrophysical Journal* 128 (1958): 664.
- Peng, T.M., Hubele, N.F., Karady, G.G., "Advancement in the application of neural networks for STLF", *IEEE Transactions on Power Systems* 7(1) (1992): 250-257.
- Rathore, B., Gupta, D. and Parashar, K., "Relation between Solar Wind Parameter and Geomagnetic Storm Condition during Cycle-23", *International Journal of Geosciences* 5(13) (2014): doi: 10.4236/ijg.2014.513131

Rumelhart, D.E., Hinton, G.E., Williams, R.J., "Learning representations by back-propagating errors" *Nature* (323) (1986): 533–536.

Singh, G. and Singh, A.K. "A study on precursors leading to geomagnetic storms using artificial neural network" *Journal of Earth System Science* 125 (2016): 899–908, <https://doi.org/10.1007/s12040-016-0702-1>

Solares, J.R.A., Wei, H.L., Boynton, R.J., Walker, S.N., Billings, S.A. "Modeling and prediction of global magnetic disturbance in near-Earth space: A case study for Kp index using NARX models", *Space Weather* 14(10) (2016): 899-916, <https://doi.org/10.1002/2016SW001463>

Stern, H.S., "Neural networks in applied statistics", *Technometrics* 38(3) (1996): 205-214.

Sugiura, M. (1964). Hourly Values of the Equatorial Dst for IGY. *Annals of the International Geophysical Year*, vol. 35. Pergamon Press, Oxford, pp. 945–948.

Takalo, J. and Timonen, J., "Neural network prediction of AE data", *Geophysical Research Letters* 24 (1997): 2403–2406, <https://doi.org/10.1029/97GL02457>

Tsurutani B.T., Gonzalez, W.D., Gonzalez, A.L.C., Guarnieri, F.L., Gopalswamy, N., Grande, M., Kamide Y., Kasahara, Y., Lu, G., Mann, I., McPherron, R., Soraas, F., Vasyliunas, V., "Corotating solar wind streams and recurrent geomagnetic activity: A review", *Journal of Geophysical Research: Space Physics* 111(A7) (2006): <https://doi.org/10.1029/2005JA011273>

Uwamahoro, J, McKinnell, L.A., and Habarulema, J.B, "Estimating the geoeffectiveness of halo CMEs from associated solar and IP parameters using neural networks", *Annales Geophysicae* 30 (2012): 963-972, [doi:10.5194/angeo-30-963-2012](https://doi.org/10.5194/angeo-30-963-2012)

Wintoft, P., Wik, M, Matzka, J., Shprits, Y., "Forecasting Kp from solar wind data: input parameter study using 3-hour averages and 3-hour range values", *J. Space Weather Space Clim.* 7 (2017): A29, <https://doi.org/10.1051/swsc/2017027>

Williams, R.J. and Zipser D., "A Learning Algorithm for Continually Running Fully Recurrent Neural Networks" *Neural Computation* 1(2) (1989): 270-280, <https://doi.org/10.1162/neco.1989.1.2.270>

Young, E.J., Moon, Y.J., Park, J., Lee, J.Y., Lee, D.H., "Comparison of neural network and support vector machine methods for Kp forecasting" *JGR Space Physics* 118(8) (2013): 5109-5117

Figures

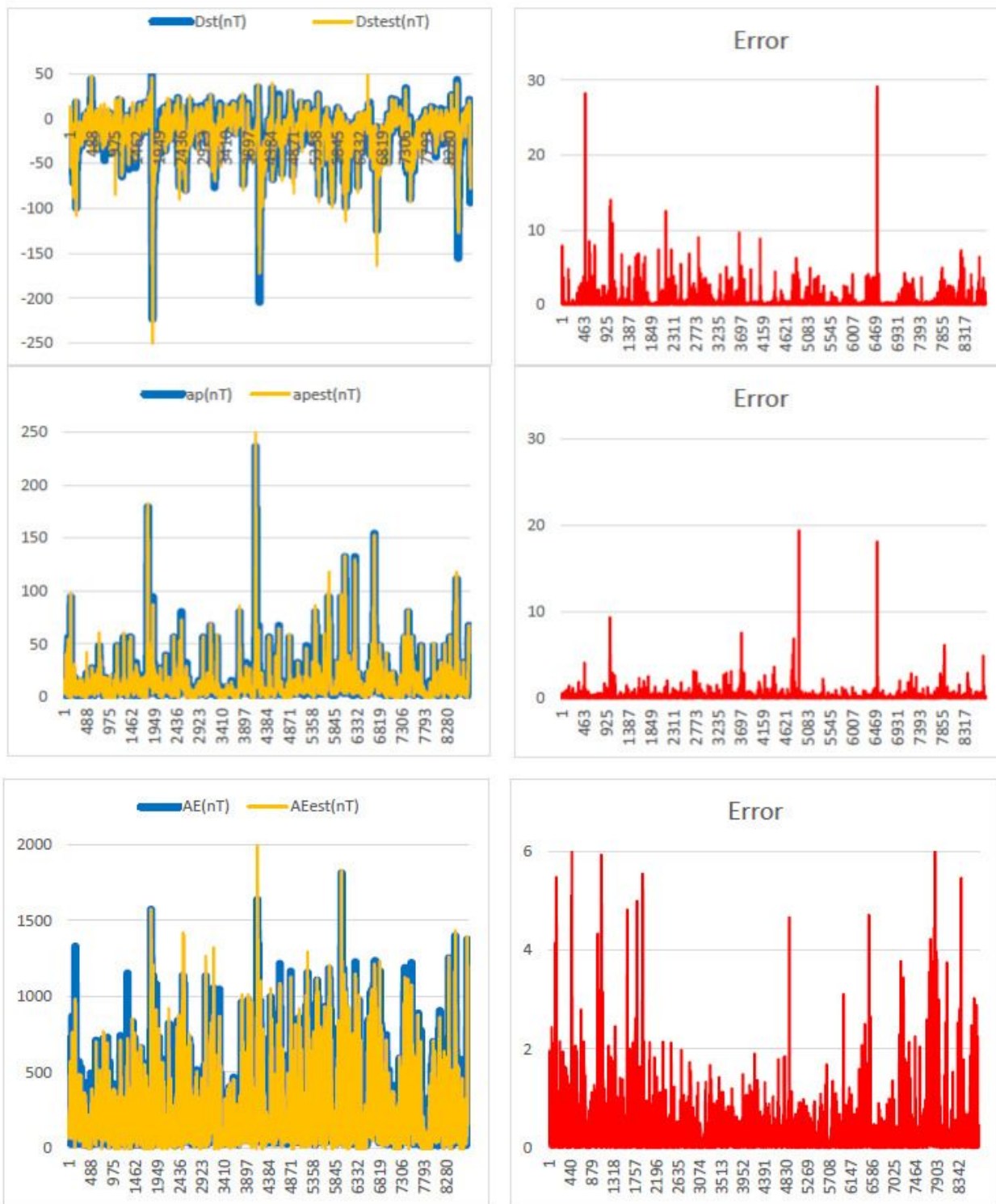


Figure 1

Annual views of the observed-estimated Dst (nT) index, ap (nT) index, AE (nT) index for 2015 year and their errors.

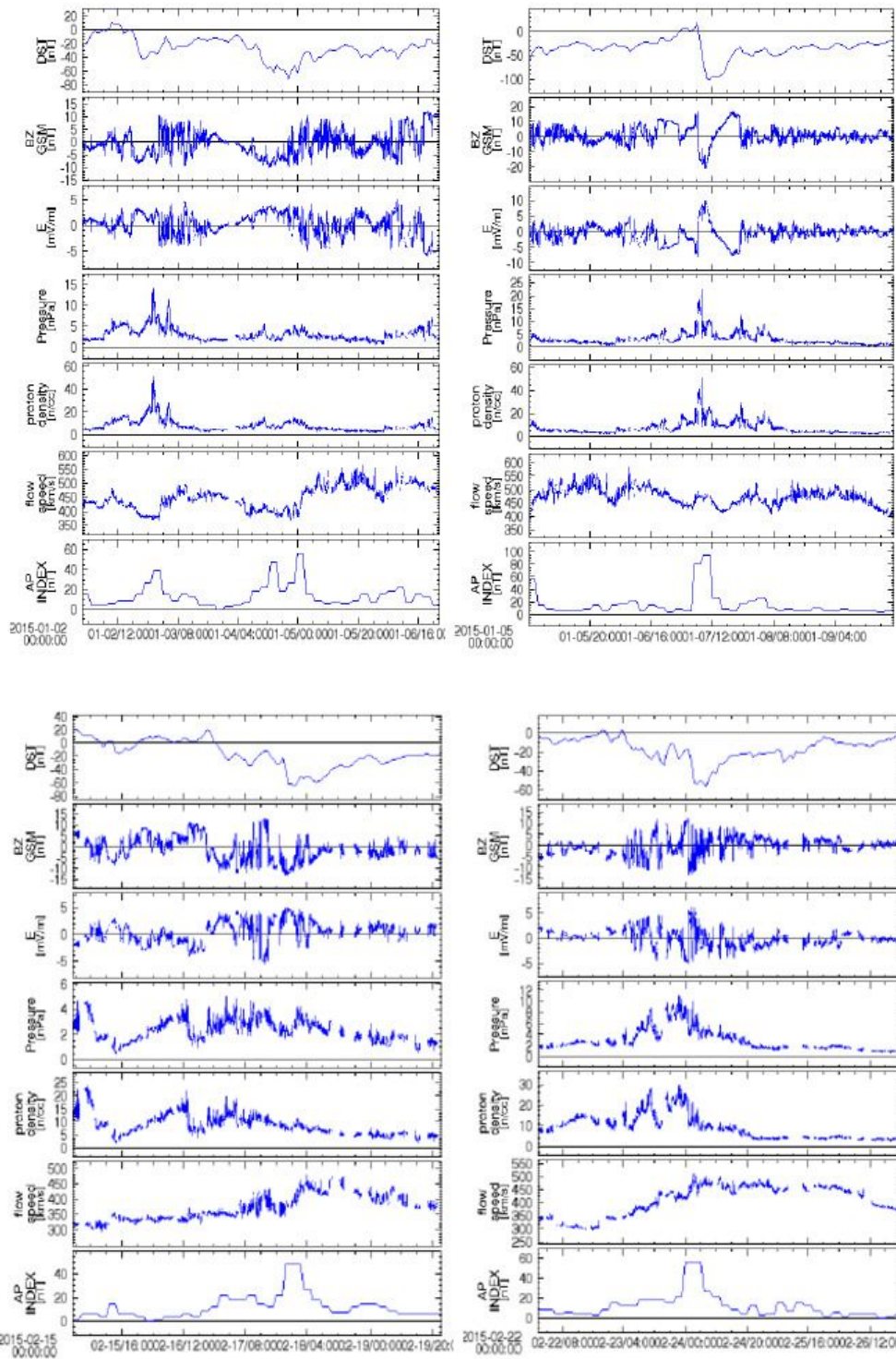


Figure 2

From top of to bottom data shown in the Dst (nT) index, the Bz magnetic field (nT), the E electric field (mV/m), the dynamic pressure P (nPa), the proton density N (1/cm³), the flow speed v (km/s) and the ap (nT) index for 2015 January 02-06 (upper left side), January 05-09 (upper right side), February 15-19 (bottom left side), and February 22-26 (bottom right side).

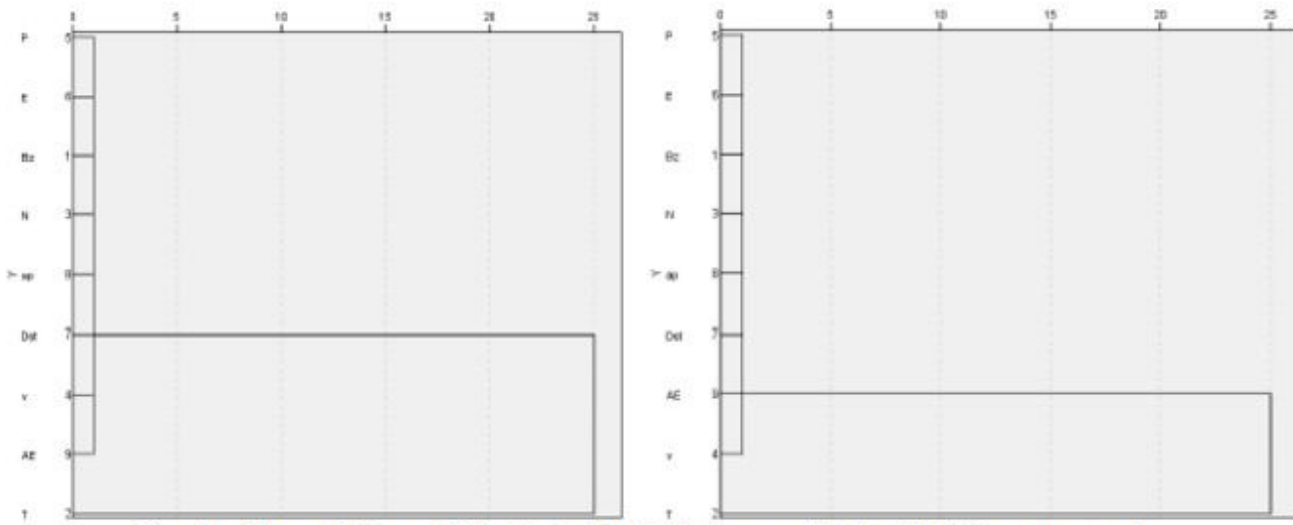


Fig. 3a. Cluster of the variables (Left-side 04 January and right-side 07 January storm).

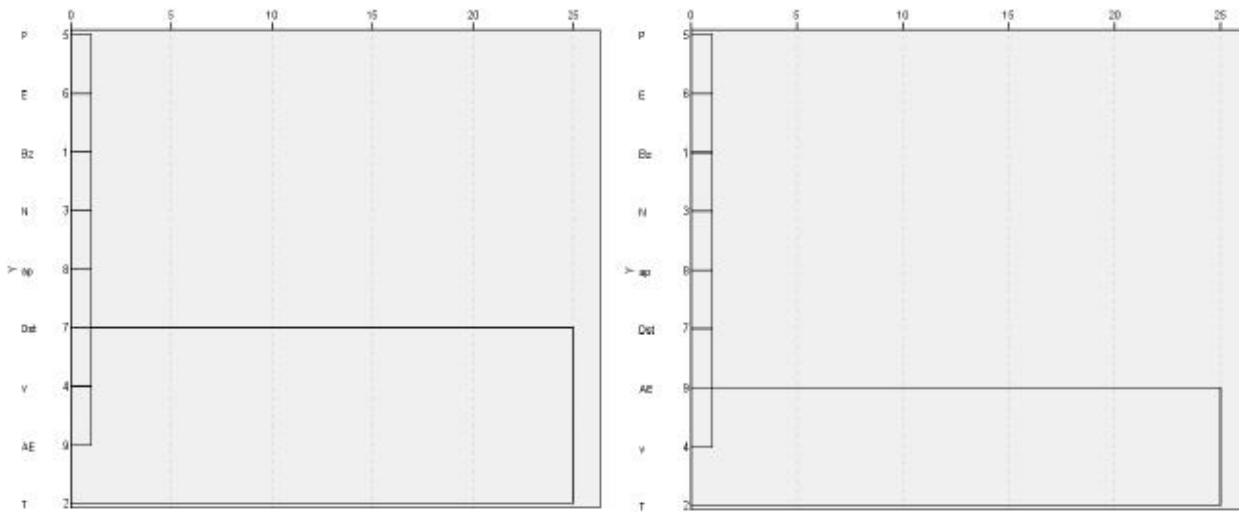


Fig. 3b. Cluster of the variables (Left-side 17 February and right-side 24 February storm).

Figure 3

a. Cluster of the variables (Left-side 04 January and right-side 07 January storm). b. Cluster of the variables (Left-side 17 February and right-side 24 February storm).

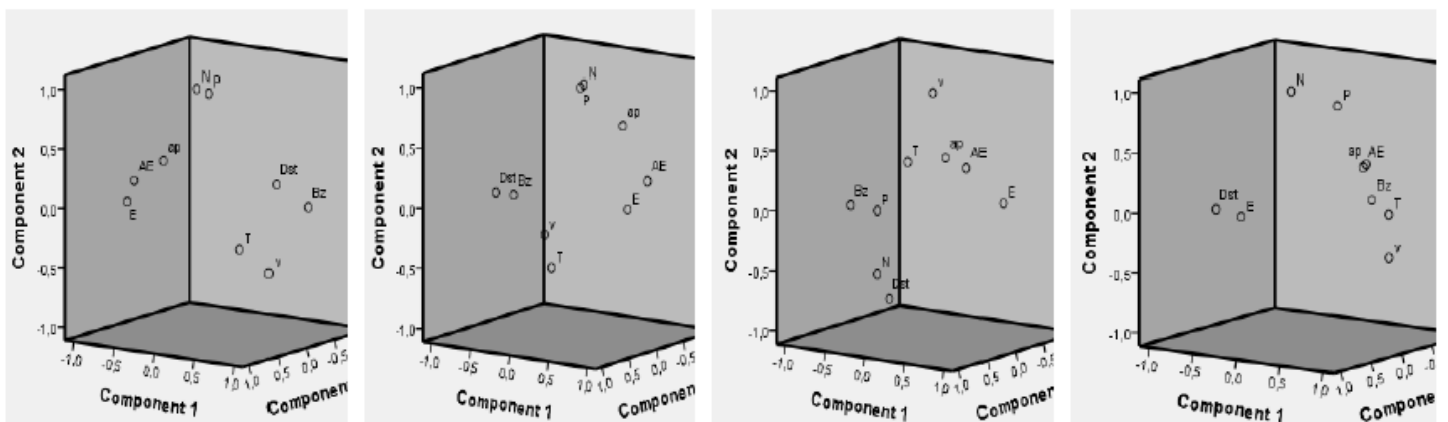


Figure 4

Scattering of the variables (From left to right 04 January, 07 January, 17 February, 24 February storms)

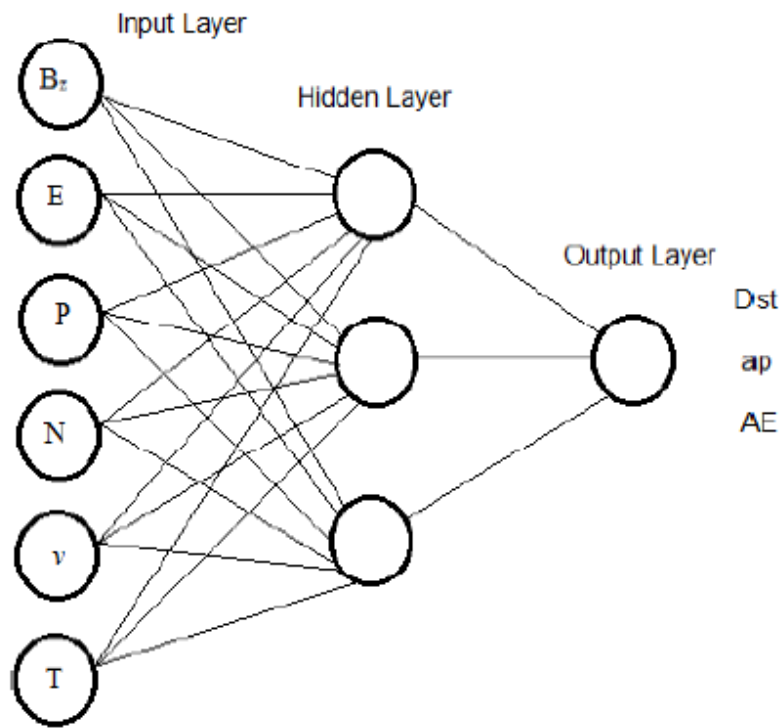


Figure 5

The neural network structure for the estimation of ZG indices

04 January 2015

07 January 2015

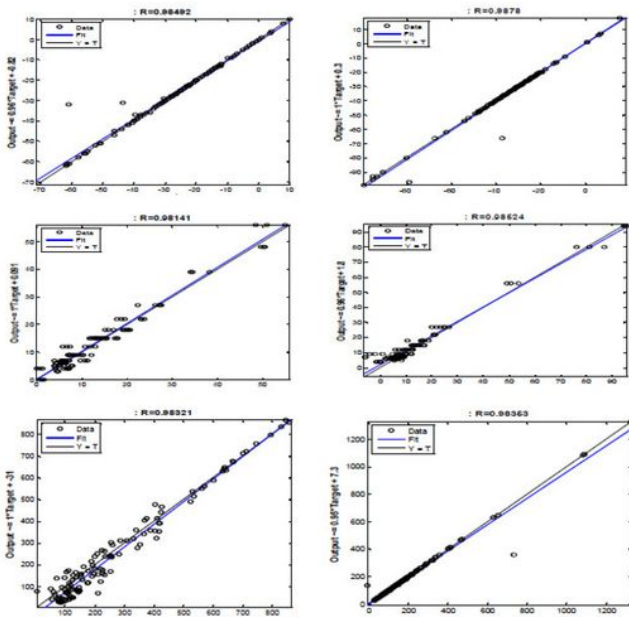


Fig. 7a. The regression plot of consistency between the estimated and observed Dst, ap, and AE (from top of to bottom) index.

17 February 2015

24 February 2015

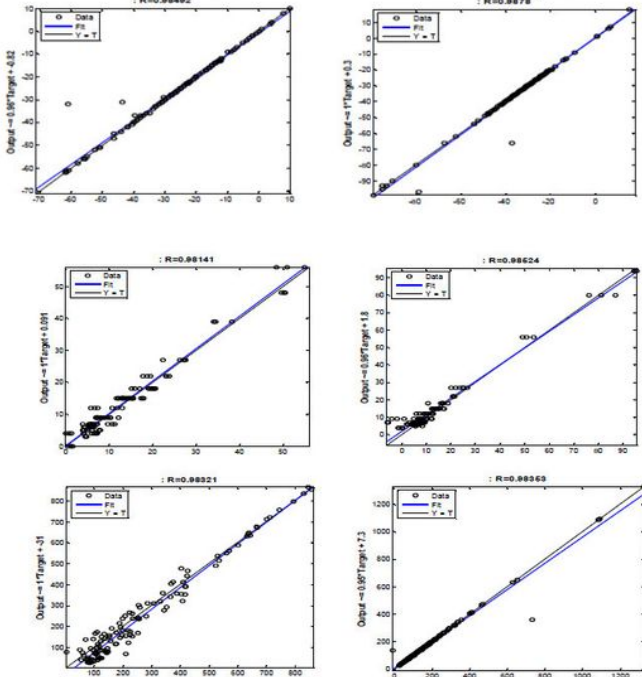


Fig. 7b. The regression plot of consistency between the estimated and observed Dst, ap, and AE (from top of to bottom) index.

Figure 7

a. The regression plot of consistency between the estimated and observed Dst, ap, and AE (from top of to bottom) index. b. The regression plot of consistency between the estimated and observed Dst, ap, and AE (from top of to bottom) index.

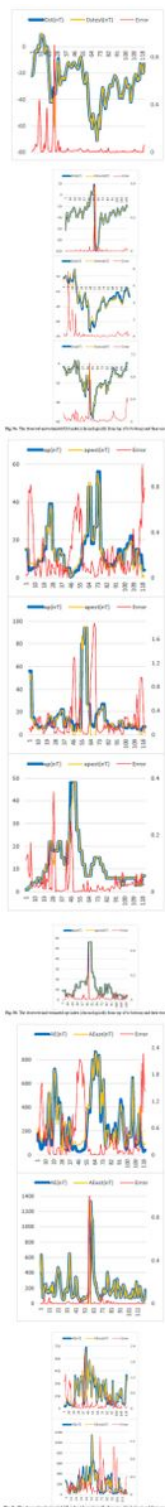


Figure 8

a. The observed and estimated Dst index (chronologically from top of to bottom) and their errors. b. The observed and estimated apt index (chronologically from top of to bottom) and their errors. c. The observed and estimated AE index (chronologically from top of to bottom) and their errors.

Supplementary Files

This is a list of supplementary files associated with this preprint. Click to download.

- [5GraphicalAbstract.png](#)